Projection-angle-dependent image intensifier distortion correction in high-speed tomography

Joaquim G. Sanctorum, Sam Van Wassenbergh, Van Nguyen, Jan De Beenhouwer, Jan Sijbers, and Joris J.J. Dirckx

***Abstract*—The geometric distortion pattern induced by electron deflection in x-ray image intensifiers is strongly influenced by the surrounding magnetic field. Therefore, variations in the magnetic field as sensed by the image intensifier causes the distortion pattern to alter accordingly, as is the case in C-arm imaging. In this work, we present a method to correct the image intensifier distortion, based on digital image correlation, and we show how this method can be efficiently used to correct for the time-varying distortion induced by an inhomogeneous distribution of ferromagnetic components in the sample rotation stage. Our experiments show that any projection recorded under an arbitrary angle can be corrected with a mean residual error below 0.48 pixels, using only three projection images of a custom reference mask sampled with a 120° angular interval to estimate the distortion behavior throughout a full rotation of the stage. As the method relies on widely available DIC software, it is very accessible and easy to use.**

***Index Terms*—image intensifier, computed tomography, distortion correction, digital image correlation, orientation-dependent**

I. Introduction

GEOMETRIC distortion is a well-known property of x-ray imaging systems utilizing image intensifiers, which is the result of two main contributions. The first contribution is the x-rays to be detected on a curved input phosphor to be subsequently projected onto a flat surface, introducing a radial stretching of the image. Secondly, the photo-electrons created and accelerated in the XRII are deflected under the influence of the surrounding magnetic field, which is mainly the Earth's magnetic field, causing a sigmoidal or "S-shaped" distortion. As the number of stereoscopic XRII-based imaging facilities is rising exponentially [1] and interest is rising in the use of XRII-based systems for low-cost tomography [2], [3], there is a need for fast and reliable distortion correction methods.

In general, an image transformation is applied to the deformed images to remove the distortion. However, the transformation to be applied is a priori unknown and during the past two decades, considerable efforts have been made to develop methods that determine a suitable correction transformation from a deformed reference input image, which is a square lattice pattern of dots in the majority of the existing correction methods. Due to the image distortion, the position of the markers will deviate from their ground truth position in the recorded images. These deviating positions are extracted from the images and related to their original positions to constitute (polynomial) dewarping functions, which are subsequently used to correct the deformed image through image resampling. Recently, a new method was developed in our lab, which is based on an entirely different principle, namely digital image correlation (DIC) [4]. This method has already been proven to be very accurate, robust and flexible.

In a typical C-arm set-up, the x-ray source and XRII rotate around the sample (e.g. a patient lying on a bench). During the rotation of the C-arm, the orientation of the XRII relative to the Earth's surface (and thus its magnetic field) is altered, causing the image distortion to be dependent on the projection angle. To solve this, various methods have been developed to estimate the distortion pattern throughout the trajectory of the XRII [5]–[7]. However, in a set-up where the XRII remains stationary, angle-dependent distortions may also arise due to an inhomogeneous distribution of ferromagnetic components in the rotation stage. In this work, we present an application of our previously developed DIC-based correction method to address such angle-dependent deformations using only a limited number of projection images for a full revolution of the stage.

II. Materials and Methods

A. Image acquisition

The radiographs are recorded using our 3DY²MOX (3D DYnamic MOrphology using X-rays) imaging system, of which the characteristics are described in [8], and can be found on the website of the project [9]. The recorded images consist of 2048 pixels × 2048 pixels covering a field of view of 292 mm × 292 mm. The maximum field of view was chosen to maximize the effect of distortion.

B. DIC-based distortion estimation

As mentioned, we used a DIC-based method to estimate the distortion pattern in the images. DIC is an optical full-field non-contact measurement technique to analyze deformations and strain behavior on the surface of objects [10]. The deformation analysis is enabled by applying a random speckle pattern to the object's surface and subsequently record a series of images of the object in its original and deformed state, yielding an image

J. G. Sanctorum and J.J.J. Dirckx are members of the Biophysics and Biomedical physics research group (BIMEF) of the University of Antwerp, Belgium. S. Van Wassenbergh is part of the Functional Morphology research group (FunMorph) of the University of Antwerp, Belgium. V. Nguyen, J. De Beenhouwer, and J. Sijbers are with the imec VisionLab research group of the University of Antwerp, Belgium. This research was funded by grant from the special research fund of the University of Antwerp (BOF-GOA 2016 33927).

series of the deformed random pattern. Through DIC analysis, the deformation of the pattern, which is assumed to be identical to the deformation of the surface, is characterized, establishing a relation between the surface coordinates of the original state and the deformed states.

In the case of image distortion, a similar relation between the original pixel positions and the distorted ones can be acquired through DIC analysis. To translate this optical technique to x-ray imaging, a random pattern of circular holes was designed and laser-cut in a sheet of stainless steel (referred to as the DIC-mask). The image of the DIC-mask recorded with an XRII will be deformed, which can be used along with the original pattern design as input for DIC analysis to readily obtain the relation between original and distorted pixel positions, which can then be used to correct the deformed images. A full description of the designed random pattern, the correction method, and the accuracy analysis can be found in [4].

C. Angle dependent correction method

Generally, image distortion can be formulated as a positional change of undistorted pixel locations, denoted as x_u and y_u:

$$\begin{aligned} x_d(x_u, y_u) &= x_u + \delta_x(x_u, y_u), \\ y_d(x_u, y_u) &= y_u + \delta_y(x_u, y_u), \end{aligned} \tag{1}$$

where the subscript d refers to the distorted position, and δ_x and δ_y are the unknown distortion surfaces, which depend on the undistorted pixel positions. Once the distortion surfaces are known, the gray values of the corrected image can be retrieved by evaluating the distorted image in the distorted coordinates:

$$I_c(x_u, y_u) = I_d\big(x_d(x_u, y_u), y_d(x_u, y_u)\big), \tag{2}$$

where I_d and I_c denote the distorted and corrected images, respectively. Generally, the distorted coordinate values x_d and y_d are non-integer, requiring interpolation of the gray values to correct the image. As described in [4], DIC analysis directly yields the distorted coordinate surfaces on a resolution of choice. In this work, these surfaces were retrieved on a 64 pixels × 64 pixels resolution for our 2048 pixels × 2048 pixels images. To obtain the intermediate values of the distorted coordinate surfaces needed to correct the images, 2D linear interpolation was used.

Once the distortion pattern is characterized by the distorted coordinate surfaces, any set of images recorded with the given set-up can be corrected for distortion. However, this statement is only true if the distortion is time-independent, which is not the case when the XRII is exposed to time-varying magnetic fields. Since the rotation of the stage is a periodic movement, the variation of the magnetic field (and thus the distortion pattern) is expected to be periodic as well. By recording a set of images of the laser-cut DIC-mask during the rotation of the stage and by analyzing the behavior of the distorted coordinate values of the pixels separately, we noticed the distortion behavior is indeed periodic for a certain image pixel. Moreover, as shown in Fig. 1, it resembles a sine function covering one period during one revolution of the stage. Based on these observations we can model the behavior of the distorted coordinate values using sinusoidal fitting:

$$\begin{aligned} x_d(\theta) &= x_0 + a_x \sin(\theta + \phi_x) \\ y_d(\theta) &= y_0 + a_y \sin\big(\theta + \phi_y\big) \end{aligned} \tag{3}$$

In this expression, θ is the projection angle. The fitting parameters x_0, y_0, a_x, a_y, ϕ_x, and ϕ_y are estimated using non-linear least-squares fitting. Due to the sinusoidal behavior of the distorted coordinates in both image directions, the distorted pixels move in elliptical trajectories over de image during the rotation of the stage. The C-arm distortion behavior as shown by Fahrig *et al*. [5] and Gutiérrez *et al.* [7] is very similar to the behavior observed in this work.

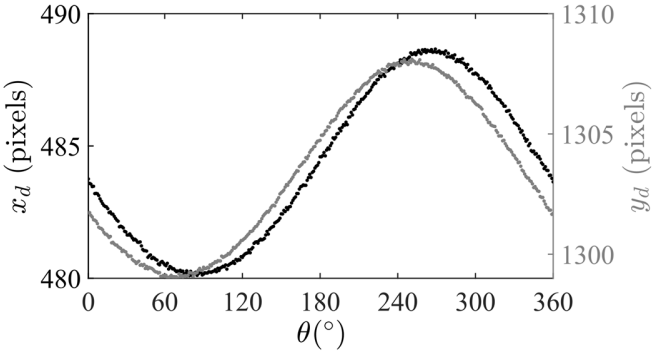

Fig. 1: Behavior of a distorted pixel position (x_d, y_d) as a function of the projection angle θ during a single revolution of the stage.

D. Experiments

For our experiments, the center of the rotation stage and the x-ray source were positioned at 264 mm and 1041 mm from the XRII, respectively. During a single revolution of the stage, we recorded 360 images using a 1° angular interval with the DIC-mask attached to the XRII, which are subsequently used in the DIC analysis to calculate the distorted coordinate surfaces. Next, we recorded 360 images of a square lattice pattern (11 × 11 grid of steel beads with a diameter of 2 mm and a center-to-center spacing of 25 mm) using the same projection angles. Then, the calculated distorted coordinate surfaces are used in two different ways. First, the surfaces are directly inserted in Eq. (2) to correct each distorted radiograph using the corresponding true distortion surfaces, which will serve as a reference. Then, a number of frames, referred to as N_{est}, are selected from this series to estimate the dynamic distortion behavior for intermediate angles using Eq. (3). These estimated distortion surfaces are subsequently used to correct the radiographs using Eq. (2).

By extracting the centroid positions of the dots after correction, and then calculating the Euclidean distance between the corrected centroid positions and their ideal positions, an estimation of the correction error can be made, as described in [4]. The standard deviation of the calculated Euclidean distances will serve as the error on the calculated means. In our experiment, we will investigate the influence of the number of projections used to estimate the distortion behavior over a single revolution of the stage on the mean and maximum error (Euclidean distance) in the corrected square lattice pattern images, denoted as R_{mean} and R_{max}, respectively. The results will be compared to those obtained by using the true corresponding distortion surfaces obtained through DIC

analysis. This way, we will deduce the minimum number of frames required to estimate the dynamic distortion behavior.

III. Results

In Fig. 2, we demonstrate the effect of the distortion correction on an image of the square lattice dot pattern. Before the correction, the distortion is clearly visible, which is shown in Fig. 2(a), whereas Fig 2(b) shows the corrected radiograph.

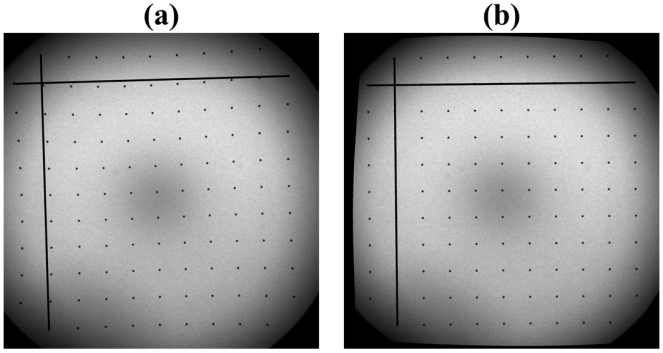

Fig. 2: (a) Original, distorted radiograph of the square lattice dot pattern. (b) Corrected radiograph of the square lattice pattern. The straight black lines drawn on the panels clearly show that the dots lie on straight lines after the correction, which corresponds to the ground truth.

A. Non-dynamic correction

For the non-dynamic correction, we used the calculated distorted coordinate surfaces of only the first image of the DIC-mask sequence to correct the distortion for the entire series of the square lattice pattern during a single revolution of the stage. Fig. 3 shows R_{mean} and R_{max} as a function of the projection angle. For images near the starting angle, the mean error is below 0.5 pixels and the maximum error is between 1 and 2 pixels. However, due to the temporal varying distortion, the mean error steeply rises slightly above 3 pixels and the maximum error rises above 10 pixels. This clearly illustrates the failure of a static correction approach.

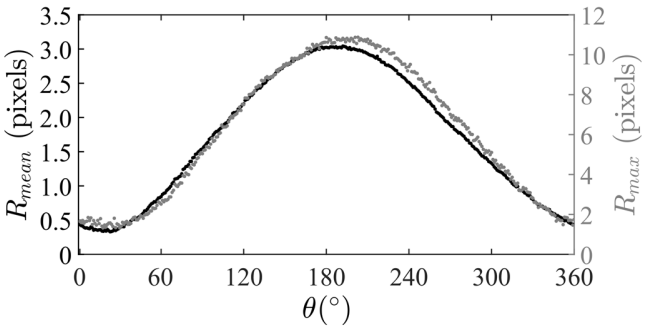

Fig. 3: Mean and maximum error (R_{mean} and R_{max} respectively) as a function of the projection angle θ for a single revolution of the stage using a static correction approach.

B. Non-dynamic correction

Next, we took into account the varying behavior of the distortion pattern by estimating the distorted coordinate values using the sinusoidal fits as defined in Eq. (3). Since three fitting parameters are present in each fit, the theoretical minimum value of N_{est} would be three. We have considered different values of $N_{est} \in [3,360]$ and selected that number of frames with equiangular intervals ($\Delta\theta$) to estimate the distortion behavior over a full revolution of the stage. Next, for each N_{est}, we corrected the full set of radiographs of the square lattice dot pattern and calculated R_{mean} and R_{max} in each frame, which are shown in Fig. 4 as a function of the projection angle θ. Regardless of N_{est}, any radiograph recorded under an arbitrary angle can be corrected with a mean residual error below 0.48 pixels and a maximum residual error below 1.66 pixels.

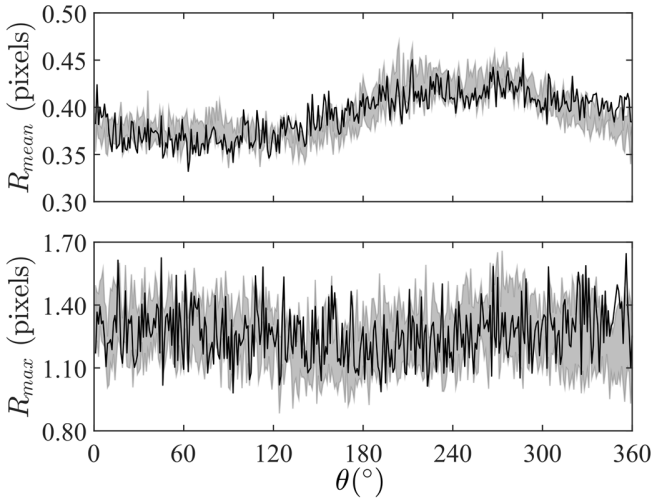

Fig. 4: The mean and maximum residual error (R_{mean} and R_{max}) as a function of the projection angle θ using a dynamic correction approach. The gray zones depict the range wherein the errors lie obtained using the different values of N_{est}, whereas the black line denotes the errors obtained using the true corresponding distortion surfaces obtained through DIC analysis.

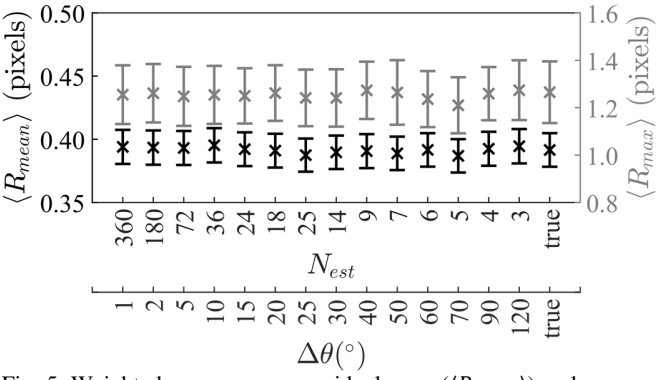

Fig. 5: Weighted average mean residual error ($\langle R_{mean} \rangle$) and average maximum error ($\langle R_{max} \rangle$) over a single revolution of the stage as a function of N_{est} or the corresponding angular interval $\Delta\theta$. The average errors obtained using the true surfaces are shown on the right.

For each value of N_{est}, we calculated the weighted average mean error and average maximum error over the 360 corrected frames, denoted as $\langle R_{mean} \rangle$ and $\langle R_{max} \rangle$, respectively. The results are shown in Fig. 5 as a function of N_{est} (or the sampling interval $\Delta\theta$). Fig. 5 shows that, regardless of N_{est}, $\langle R_{mean} \rangle$ lies below 0.40 pixels, whereas $\langle R_{max} \rangle$ lies between 1.2 pixels and 1.4 pixels. Moreover, for each N_{est}, the average values are very

similar and an ANOVA test showed that none of the datasets have significantly different averages.

IV. Discussion

This work aimed at presenting a projection-angle-dependent distortion correction method for XRII-based imaging. Since there is a large variety of used equipment and imaging conditions, it is appropriate to express our results in units of distance instead of pixels to compare our work to previously developed methods. Fig. 4 shows that any radiograph recorded under an arbitrary angle can be corrected with a mean residual error below 0.48 pixels, which corresponds to 0.068 mm as our images consist of 2048 pixels × 2048 pixels covering a field of view of 292 mm × 292 mm (the diameter of the XRII is 14"). Fig. 5 shows that the weighted average mean residual error is around 0.39 pixels, regardless of the sampling interval, which corresponds to 0.056 mm. As the ANOVA test showed no significant difference between the datasets, three images sampled with an angular interval of 120° are sufficient to accurately estimate the full dynamic behavior during a single revolution of the stage.

One of the earliest dynamic correction methods was introduced by Fahrig *et al.* [5]., who obtained mean residual errors of 0.039 mm for a field of view of 246 mm × 246 mm by sampling recordings of a square lattice pattern reference mask using an angular interval of 2°. To estimate the distortion for intermediate angles, linear interpolation was used. This result seems more accurate than ours, but the field of view is considerably smaller, implying less strong distortion. Liu *et al.* [6] used a similar approach, but instead of linear interpolation between the data points, they used polynomial fitting, reaching an accuracy of 0.048 mm using a sampling interval of 5° to 10° for a 225 mm × 225 mm field of view. Gutiérrez *et al.* [7] used a sampling interval of 30° to obtain an accuracy of 0.142 mm for a 330 mm × 330 mm field of view. This was done by first smoothing the trajectories of the distorted pixel coordinates before applying polynomial fitting. Compared to these results, our correction method blends in, as the average accuracy, as well as the size of the field of view, fall in between. Our method stands out from the rest due to the sampling interval of 120° and the need for only three images to estimate the full 360° behavior of the varying distortion.

As recording radiographs and subsequent distortion correction are the first steps in the CT-chain, an inaccurate correction method can result in the accumulation of errors in further processing steps, such as system calibration and tomographic reconstruction, which will be the topic of our future research. Therefore, users of XRII-based tomographic systems are advised to dynamically correct for the distortion, as they might be unaware of the presence of ferromagnetic components in rotating parts of their set-up.

V. Conclusion

We have presented an application of a DIC-based distortion correction method for XRII-based tomography purposes. Our experiments show that, based on only three projection images sampled using a 120° angular interval, the full 360° behavior of the distortion could be corrected with a mean residual error smaller than 0.48 pixels for each frame. An ANOVA test showed that this large sampling interval could be used without accuracy loss. As DIC software is widely available, the method is very accessible and easy to use.

Acknowledgements

The authors would like to acknowledge William Deblauwe and Wim Huyge for the construction of the rotation stage. This research is funded by a grant from the special research fund of the University of Antwerp (BOF-GOA 2016 33927).

References

[1] D. Orenstein, "Brown's influential biomechanics X-ray technology grows ever more powerful." https://phys.org/news/2016-12-brown-influential-biomechanics-x-ray-technology.html (accessed Mar. 17, 2020).

[2] C. de Molina, J. Pascau, M. Desco, and M. Abella, "Calibration of a C-arm X-Ray System for Its Use in Tomography," in *XIII Mediterranean Conference on Medical and Biological Engineering and Computing 2013*, Cham, 2014, pp. 245–248, doi: 10.1007/978-3-319-00846-2_61.

[3] M. Abella, C. de Molina, N. Ballesteros, A. García-Santos, Á, Martínez, "Enabling tomography with low-cost C-arm systems," *PLOS ONE*, vol. 13, no. 9, p. e0203817, Sep. 2018, doi: 10.1371/journal.pone.0203817.

[4] J. G. Sanctorum, S. Van Wassenbergh, P. Aerts, and J. J. J. Dirckx, "Technical Note: Correction of geometric x-ray image intensifier distortion based on digital image correlation," *Med. Phys.*, vol. 47, no. 2, pp. 597–603, 2020, doi: 10.1002/mp.13944.

[5] R. Fahrig, M. Moreau, and D. W. Holdsworth, "Three-dimensional computed tomographic reconstruction using a C-arm mounted XRII: Correction of image intensifier distortion," *Med. Phys.*, vol. 24, no. 7, pp. 1097–1106, Jul. 1997, doi: 10.1118/1.598013.

[6] R. R. Liu, S. Rudin, and D. R. Bednarek, "Super-global distortion correction for a rotational C-arm x-ray image intensifier," *Med. Phys.*, vol. 26, no. 9, pp. 1802–1810, 1999, doi: 10.1118/1.598684.

[7] L. F. Gutiérrez, C. Ozturk, E. R. McVeigh, and R. J. Lederman, "A practical global distortion correction method for an image intensifier based x-ray fluoroscopy system," *Med. Phys.*, vol. 35, no. 3, pp. 997–1007, Feb. 2008, doi: 10.1118/1.2839099.

[8] J. G. Sanctorum, D. Adriaens, J.J.J. Dirckx, J. Sijbers, C. Van Ginneken, P. Aerts, S. Van Wassenbergh, "Methods for characterization and optimisation of measuring performance of stereoscopic x-ray systems with image intensifiers," *Meas. Sci. Technol.*, 2019, doi: 10.1088/1361-6501/ab23e7.

[9] "Technical information - 3-Dimensional DYnamic MOrphology using X-rays (3D2YMOX) - University of Antwerp." https://www.uantwerpen.be/en/research-groups/3d2ymox/technical-information/ (accessed Jan. 06, 2020).

[10] M. A. Sutton, J.-J. Orteu, and H. Schreier, *Image Correlation for Shape, Motion and Deformation Measurements*. Boston, MA: Springer US, 2009.